

Efficient Joint Resource Allocation for Wireless Powered ISAC with Target Localization

Boyao Li[†], Qinwei He[‡], Boao Zhang[†], Xiaopeng Yuan^{†*} and Anke Schmeink[†]

[†]INDA Chair, RWTH Aachen University, Germany, Email: li|yuan|schmeink@inda.rwth-aachen.de

[‡]Global Energy Interconnection Research Institute Europe GmbH, Germany, Email: qinwei.he@geiri.eu

Abstract—Integrated sensing and communication (ISAC) enables 6G networks to share radio resources for sensing and data transmission. For energy-limited ISAC systems, wireless power transfer (WPT) can be integrated as a power supply, which also introduces tradeoffs among harvested energy, communication throughput, and sensing accuracy. Motivated by this, we study a wireless powered multi-user ISAC system for multi-target localization, where a base station (BS) broadcasts a WPT signal for energy harvesting and users then transmit data with the harvested energy to the BS sequentially. Meanwhile, both the WPT signal and the users' data signals are exploited for target localization at the BS. By imposing Cramér-Rao bound (CRB) constraints to guarantee localization accuracy, we formulate a minimum user throughput maximization problem that jointly optimizes the WPT duration, per-user transmission durations, and user transmit powers. To address the variable coupling and inherent nonconvexity of the problem, we derive a more tractable reformulation via variable substitutions and logarithmic objective transformations. Since the CRB constraints remain nonconvex, we further develop a successive convex approximation (SCA)-based iterative algorithm and finally obtain an efficient suboptimal solution. Numerical results demonstrate the algorithm convergence and significant performance gains of the proposed scheme over benchmark schemes, highlighting the importance of joint resource allocation design for wireless powered ISAC systems.

Index Terms—Integrated sensing and communication (ISAC), wireless power transfer (WPT), target localization, Cramér-Rao bound (CRB), efficient resource allocation.

I. INTRODUCTION

Integrated sensing and communication (ISAC) has emerged as a key pillar of 6G wireless networks, enabling high-quality wireless connectivity and accurate sensing capability within a unified infrastructure [1]. By sharing spectrum and hardware, ISAC is expected to support diverse applications such as smart home, human-computer interaction, and vehicle-to-everything (V2X) [2]. This tight integration, however, also introduces tradeoffs between sensing and communication due to shared limited resources.

To navigate these tradeoffs, extensive research efforts have been devoted to ISAC, e.g., in waveform design [3], [4] and advanced multiple access schemes [5]. In accordance with

different sensing demands, various sensing tasks have been studied, including detection, estimation, and recognition [6]. In particular, target localization, as a representative estimation task, is crucial for location-aware services such as indoor navigation and tracking. This has spurred increasing interest in localization-oriented ISAC, e.g., in cooperative networks [7] and unmanned aerial vehicle (UAV)-assisted scenarios [8].

Despite its potential, ISAC deployment becomes challenging in energy-limited scenarios. To address this challenge, wireless power transfer (WPT), by harvesting energy from ambient or dedicated radio frequency (RF) signals, has become a natural solution to enable sustainable ISAC operation for batteryless devices [9], [10]. Under a finite time budget, extending the WPT phase increases the harvested energy, but inevitably reduces the available time for the subsequent ISAC phase. To optimize this tradeoff, efficient resource allocation is crucial to orchestrate the energy-communication-localization interplay in wireless powered ISAC systems.

To this end, several works have investigated resource allocation for wireless powered ISAC. In [11], the authors jointly optimize power control as well as WPT and ISAC beamforming to improve sensing performance while guaranteeing the communication requirements. In addition, [12] investigates a UAV-enabled wireless powered ISAC system and jointly optimizes the filter and waveform design, time scheduling and uplink powers of users, and UAV trajectory. However, these designs do not explicitly consider the target localization as the sensing task. Their sensing objectives are characterized by nonspecific metrics such as signal-to-interference-plus-noise ratio (SINR), rather than localization-specific metrics such as Cramér-Rao bound (CRB) that directly quantifies localization accuracy. Moreover, they do not fully exploit the sensing opportunities from all phases and nodes, and thus cannot leverage the sensing geometry required for accurate localization. Consequently, the potential gains from WPT-ISAC co-design and CRB-constrained resource allocation remain insufficiently explored.

To fill this gap, we study a wireless powered multi-user ISAC system, where the base station (BS) first performs WPT to energize the users, and then users transmit data to the BS with the obtained energy, while both phases jointly contribute to the multi-target localization task guaranteed via CRB constraints. The main contributions of this paper are summarized as follows:

The work was supported in part by BMFTR Germany in the projects 6G-RIC under Grant 16KISK028, 6GEM+ under Grant 16KIS2409K, and GEM-X under Grant 16KISS004K, and in part by the State Grid Corporation of China under Grant 5700-202358798A-3-9-HW.

*X. Yuan is the corresponding author.

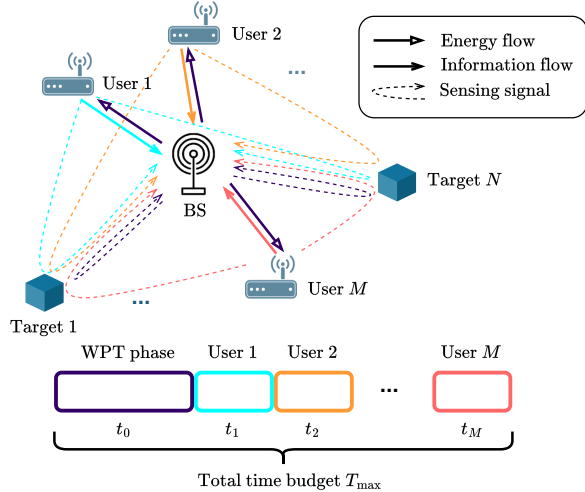


Fig. 1. Illustration of a wireless powered M -user ISAC system with N targets under a total time budget T_{\max} .

- Localization-specific wireless powered ISAC framework:** We propose a two-phase WPT-ISAC protocol for multi-target localization in energy-limited systems, where the localization geometry and opportunities are fully considered and exploited. Under this design, we formulate a max-min throughput problem by jointly optimizing the WPT duration, per-user transmission time and power, subject to energy causality and per-target CRB-based localization accuracy constraints. The formulation explicitly captures the tradeoffs among harvested energy, communication performance, and localization accuracy.
- Efficient joint resource allocation:** To tackle the resulting nonconvex time-power coupled problem with intricate CRB constraints, we develop an equivalent reformulation via variable substitutions and logarithmic transformations, which removes the multiplicative coupling. After the reformulation, we construct convex surrogates for the remaining nonconvexity in CRB constraints and propose an efficient successive convex approximation (SCA)-based iterative algorithm to obtain a high-quality suboptimal solution.
- Numerical investigation:** Numerical results demonstrate fast convergence of the iterative algorithm and significant throughput gains of the proposed scheme over benchmark schemes, and provide insights into how resources can be jointly allocated to balance heterogeneous performance requirements in wireless powered ISAC systems.

The rest of this paper is organized as follows. In Section II, we introduce the system model and the CRB model, and formulate the optimization problem. Section III develops the proposed iterative algorithm. Numerical results are presented in Section IV, and conclusions are drawn in Section V.

II. PROBLEM FORMULATION

A. System Model

We consider a wireless powered ISAC system consisting of M batteryless users, N passive targets, and a BS located

at $\mathbf{x}_0 \in \mathbb{R}^2$, as shown in Fig. 1. The position of user $m \in \mathcal{M} \triangleq \{1, \dots, M\}$ is denoted by $\mathbf{x}_m \in \mathbb{R}^2$, while the reference position of target $n \in \mathcal{N} \triangleq \{1, \dots, N\}$ is denoted by $\mathbf{q}_n \in \mathbb{R}^2$. The users aim to transmit data to the BS, while the BS is required to localize the passive targets based on the received sensing signals.

In the WPT phase, the BS broadcasts an energy-carrying signal with power p_0 over a duration t_0 , from which all users harvest energy for the subsequent ISAC phase. The harvested energy at user m is given by

$$E_m(t_0) = \zeta_m h_m t_0 p_0, \quad \forall m \in \mathcal{M}, \quad (1)$$

where ζ_m is the energy conversion efficiency of user m and h_m denotes the channel gain from the BS to user m .

After the WPT phase, the system enters an ISAC phase consisting of M slots. In the m -th slot, user m transmits an information-bearing waveform with power p_m over a duration t_m , which simultaneously supports target localization and uplink communication.

During the ISAC phase, while illuminating the targets for sensing, user m simultaneously transmits its data to the BS. In slot m , the signal-to-noise ratio (SNR) at the BS is

$$\gamma_m(p_m) = \frac{p_m h_m}{\sigma^2}, \quad \forall m \in \mathcal{M}. \quad (2)$$

The achievable throughput of user m for a transmission duration t_m is expressed as

$$R_m(t_m, p_m) = t_m W \log_2(1 + \gamma_m(p_m)), \quad \forall m \in \mathcal{M}. \quad (3)$$

The total transmission duration of the WPT phase and all ISAC slots is constrained by a total time budget T_{\max} , i.e.,

$$\sum_{m=0}^M t_m \leq T_{\max}. \quad (4)$$

Since the transmission of batteryless user m is solely powered by the harvested energy $E_m(t_0)$, the following energy causality constraint must hold:

$$t_m p_m \leq E_m(t_0), \quad \forall m \in \mathcal{M}. \quad (5)$$

Furthermore, due to hardware limitations, the transmit power of each user is bounded by

$$0 < p_m \leq P_{\max}, \quad \forall m \in \mathcal{M}. \quad (6)$$

B. CRB-Based Localization Model

To quantify the target localization accuracy, we adopt a CRB-based localization model. Both the WPT signal and the users' ISAC signals illuminate all targets, which then backscatter the incident energy toward the BS. The BS receives the echo signals and processes them to estimate the target positions. Thus, each user provides a distinct bistatic sensing geometry, while the BS provides a monostatic geometry for localization.

For each target $n \in \mathcal{N}$, we characterize both the bistatic and monostatic sensing geometries. The bistatic round-trip

distance in slot m is given by

$$r_{m,n} = \|\mathbf{x}_m - \mathbf{q}_n\| + \|\mathbf{x}_0 - \mathbf{q}_n\|, \quad \forall m \in \mathcal{M}, \quad \forall n \in \mathcal{N}, \quad (7)$$

while the monostatic round-trip distance is

$$r_{0,n} = 2\|\mathbf{x}_0 - \mathbf{q}_n\|, \quad \forall n \in \mathcal{N}. \quad (8)$$

Taking the gradient of $r_{m,n}$ with respect to the reference target location \mathbf{q}_n yields

$$\nabla_{\mathbf{q}_n} r_{m,n} = \begin{cases} -\frac{\mathbf{x}_m - \mathbf{q}_n}{\|\mathbf{x}_m - \mathbf{q}_n\|} - \frac{\mathbf{x}_0 - \mathbf{q}_n}{\|\mathbf{x}_0 - \mathbf{q}_n\|}, & m \in \mathcal{M}, \\ -2\frac{\mathbf{x}_0 - \mathbf{q}_n}{\|\mathbf{x}_0 - \mathbf{q}_n\|}, & m = 0, \end{cases} \quad (9)$$

$$\triangleq \begin{bmatrix} X_{m,n} \\ Y_{m,n} \end{bmatrix}, \quad \forall m \in \mathcal{M} \cup \{0\}, \quad \forall n \in \mathcal{N}.$$

Following the classical CRB analysis for range-based target localization [13], [14], the obtained gradient terms in (9) are used to construct the Fisher information matrix (FIM) associated with target $n \in \mathcal{N}$, which can be expressed as

$$\mathbf{J}_n = \sum_{m=0}^M p_m K_{m,n} \begin{bmatrix} X_{m,n}^2 & X_{m,n} Y_{m,n} \\ X_{m,n} Y_{m,n} & Y_{m,n}^2 \end{bmatrix}, \quad (10)$$

where the scaling factor $K_{m,n}$ is defined as

$$K_{m,n} = \frac{8\pi^2 W^2 h_{m,n}}{\sigma^2 c^2}, \quad \forall m \in \mathcal{M} \cup \{0\}, \quad \forall n \in \mathcal{N}. \quad (11)$$

Here, W denotes the effective bandwidth, $h_{m,n}$ denotes the channel gain from transmitter m to target n , with $m = 0$ corresponding to the BS and $m \in \mathcal{M}$ corresponding to the users. Moreover, σ^2 is the noise power at the BS and c is the speed of light.

For notational convenience, the FIM associated with target n in (10) is rewritten in the compact form:

$$\mathbf{J}_n = \begin{bmatrix} A_n & C_n \\ C_n & B_n \end{bmatrix}, \quad \forall n \in \mathcal{N}, \quad (12)$$

where

$$A_n = \sum_{m=0}^M p_m K_{m,n} X_{m,n}^2, \quad B_n = \sum_{m=0}^M p_m K_{m,n} Y_{m,n}^2, \quad (13)$$

$$C_n = \sum_{m=0}^M p_m K_{m,n} X_{m,n} Y_{m,n}.$$

Under non-degenerate localization geometry, the FIM is positive definite, i.e., $A_n B_n - C_n^2 > 0$ and the CRB matrix can be expressed as the inverse of FIM:

$$\mathbf{J}_n^{-1} = \frac{1}{A_n B_n - C_n^2} \begin{bmatrix} B_n & -C_n \\ -C_n & A_n \end{bmatrix}, \quad \forall n \in \mathcal{N}. \quad (14)$$

The trace of the CRB matrix represents a lower bound for the target location estimation and is given by

$$\text{tr}(\mathbf{J}_n^{-1}) = \frac{A_n + B_n}{A_n B_n - C_n^2}, \quad \forall n \in \mathcal{N}. \quad (15)$$

Given a required localization accuracy threshold $\eta > 0$, the following constraint must be satisfied:

$$\text{tr}(\mathbf{J}_n^{-1}) \leq \eta, \quad \forall n \in \mathcal{N}. \quad (16)$$

To maximize the communication performance while ensuring fairness among all users, the minimum achievable throughput is adopted as the optimization objective. Accordingly, the overall optimization problem is formulated as

$$(\mathcal{P}1): \max_{\mathbf{t}, \mathbf{p}} \min_{m \in \mathcal{M}} \{R_m(t_m, p_m)\} \quad (17a)$$

$$\text{s.t. } t_m > 0, \quad \forall m \in \mathcal{M} \cup \{0\},$$

$$(4), (5), (6), (16),$$

where $\mathbf{t} \triangleq [t_0, t_1, \dots, t_M]^T \in \mathbb{R}^{M+1}$ collects the transmit durations of the BS and all users. Problem (P1) is nonconvex since $R_m(t_m, p_m)$ is not jointly concave in (t_m, p_m) and nonconvex constraints (5) and (16) involve multiplicative couplings among the optimization variables. As a result, problem (P1) cannot be directly solved using standard convex optimization techniques.

III. PROPOSED ITERATIVE SOLUTION

This section develops an efficient iterative algorithm to solve (P1). We first reformulate (P1) via variable substitutions and logarithmic transformations, and then apply SCA to handle the remaining nonconvexity.

A. Problem Reformulation

To handle the multiplicative coupling between t_m and p_m in constraints (5) and (16), we apply a logarithmic change of variables by replacing (t_m, p_m) with (u_m, v_m) as

$$u_m = \log(t_m), \quad v_m = \log(p_m), \quad \forall m \in \mathcal{M}, \quad (18)$$

which guarantees $t_m > 0$ and $p_m > 0$ automatically. Under this substitution, the energy causality constraint (5) becomes

$$u_m + v_m \leq \log(E_m(t_0)), \quad \forall m \in \mathcal{M}, \quad (19)$$

which converts the original product terms $t_m p_m$ into a linear term. Moreover, since $E_m(t_0)$ in (1) is affine in t_0 , $\log(E_m(t_0))$ is concave in t_0 , and thus constraint (19) is convex. Also, with variable replacement, the throughput (3) transforms to

$$\tilde{R}_m(u_m, v_m) = e^{u_m} W \log_2 \left(1 + \frac{h_m}{\sigma^2} e^{v_m} \right), \quad \forall m \in \mathcal{M}, \quad (20)$$

which is still not jointly concave in (u_m, v_m) .

To overcome this difficulty, we apply a logarithmic transformation to $\tilde{R}_m(u_m, v_m)$, inspired by a similar technique to that in our prior works [15], [16]. Since the logarithm is strictly increasing, maximizing $\tilde{R}_m(u_m, v_m)$ is equivalent to maximizing $\log \tilde{R}_m(u_m, v_m)$, which can be expressed as

$$\log \tilde{R}_m(u_m, v_m) \quad (21)$$

$$= u_m + \log(W) + \log \left(\log_2 \left(1 + \frac{h_m}{\sigma^2} e^{v_m} \right) \right), \quad \forall m \in \mathcal{M}.$$

The first term is affine in u_m and $\log(W)$ is a constant, while the last term is concave in v_m , as established in the following lemma.

Lemma 1. For any $h_m > 0$ and $\sigma^2 > 0$, the function

$$f(v_m) = \log \left(\log_2 \left(1 + \frac{h_m}{\sigma^2} e^{v_m} \right) \right) \quad (22)$$

is strictly concave in $v_m \in \mathbb{R}$.

Proof. To prove the concavity of $f(v_m)$, we define $k_m = \frac{h_m}{\sigma^2} > 0$ and $g(v_m) = 1 + k_m e^{v_m} > 1$. Using the identity $\log_2 g(v_m) = \frac{\log g(v_m)}{\log 2}$, the function $f(v_m)$ becomes

$$f(v_m) = \log(\log g(v_m)) - \log(\log 2). \quad (23)$$

The first derivative of $f(v_m)$ is therefore

$$f'(v_m) = \frac{k_m e^{v_m}}{g(v_m) \log g(v_m)}. \quad (24)$$

Differentiating once more yields

$$\begin{aligned} f''(v_m) &= \frac{k_m e^{v_m} (g(v_m) \log g(v_m) - k_m e^{v_m} (\log g(v_m) + 1))}{g(v_m)^2 (\log g(v_m))^2} \\ &= \frac{k_m e^{v_m} (\log g(v_m) - k_m e^{v_m})}{g(v_m)^2 (\log g(v_m))^2}, \end{aligned} \quad (25)$$

Since $g(v_m) > 1$, using the well-known inequality

$$\log(y) < y - 1, \quad \forall y > 1, \quad (26)$$

we have

$$\log g(v_m) < g(v_m) - 1 = k_m e^{v_m}. \quad (27)$$

Hence, the numerator of $f''(v_m)$ is negative, while the denominator is positive, and therefore $f''(v_m) < 0$ for all $v_m \in \mathbb{R}$, which completes the proof. \square

Consequently, $\log \tilde{R}_m(u_m, v_m)$ is jointly concave in (u_m, v_m) , as the sum of an affine function in u_m and a concave function in v_m . Moreover, the objective function $\min_{m \in \mathcal{M}} \{\log \tilde{R}_m(u_m, v_m)\}$ is concave as the pointwise minimum of concave functions.

As for CRB constraint (16), since $A_n B_n - C_n^2 > 0$, the above inequality can be rewritten as

$$A_n + B_n - \eta(A_n B_n - C_n^2) \leq 0, \quad \forall n \in \mathcal{N}. \quad (28)$$

To reveal the algebraic structure of $A_n B_n - C_n^2$ and its dependence on the power variables $\{p_m\}$, for each $n \in \mathcal{N}$, we define $a_{m,n} = \sqrt{p_m K_{m,n}} X_{m,n}$, $b_{m,n} = \sqrt{p_m K_{m,n}} Y_{m,n}$. With these definitions, $A_n = \sum_{m=0}^M a_{m,n}^2$, $B_n = \sum_{m=0}^M b_{m,n}^2$, and $C_n = \sum_{m=0}^M a_{m,n} b_{m,n}$. Applying

Lagrange identity, we obtain

$$\begin{aligned} A_n B_n - C_n^2 &= \frac{1}{2} \sum_{i=0}^M \sum_{j=0}^M (a_{i,n} b_{j,n} - a_{j,n} b_{i,n})^2 \\ &= \frac{1}{2} \sum_{i=0}^M \sum_{j=0}^M p_i p_j K_{i,n} K_{j,n} (X_{i,n} Y_{j,n} - X_{j,n} Y_{i,n})^2. \end{aligned} \quad (29)$$

By substituting (29) and separating the terms involving the fixed BS power p_0 , the CRB constraint (28) can be equivalently reformulated as

$$\begin{aligned} F_n(\mathbf{p}) &= \sum_{m=1}^M \alpha_{m,n} p_m + \mu_n - \frac{\eta}{2} \sum_{i=1}^M \sum_{j=1}^M \beta_{i,j,n} p_i p_j \\ &\quad - \eta p_0 \sum_{m=1}^M \varphi_{m,n} p_m \leq 0, \quad \forall n \in \mathcal{N}, \end{aligned} \quad (30)$$

where $\mathbf{p} \triangleq [p_1, \dots, p_M]^T$ denotes the vector of transmit powers. The coefficients for each $n \in \mathcal{N}$ are defined as

$$\alpha_{m,n} \triangleq K_{m,n} (X_{m,n}^2 + Y_{m,n}^2), \quad m \in \mathcal{M}, \quad (31)$$

$$\mu_n \triangleq p_0 K_{0,n} (X_{0,n}^2 + Y_{0,n}^2), \quad (32)$$

$$\beta_{i,j,n} \triangleq K_{i,n} K_{j,n} (X_{i,n} Y_{j,n} - X_{j,n} Y_{i,n})^2, \quad i, j \in \mathcal{M}, \quad (33)$$

$$\varphi_{m,n} \triangleq K_{0,n} K_{m,n} (X_{0,n} Y_{m,n} - X_{m,n} Y_{0,n})^2, \quad m \in \mathcal{M}. \quad (34)$$

Replacing the optimization variables, (30) can be written as

$$\begin{aligned} \tilde{F}_n(\mathbf{v}) &= \sum_{m=1}^M \alpha_{m,n} e^{v_m} + \mu_n - \frac{\eta}{2} \sum_{i=1}^M \sum_{j=1}^M \beta_{i,j,n} e^{v_i + v_j} \\ &\quad - \eta p_0 \sum_{m=1}^M \varphi_{m,n} e^{v_m}, \quad \forall n \in \mathcal{N}. \end{aligned} \quad (35)$$

While the first term is convex in \mathbf{v} and μ_n is constant, the last two terms are concave because $e^{v_i + v_j}$ and e^{v_m} are convex in \mathbf{v} , and the negative of a convex function is concave. Thus, $\tilde{F}_n(\mathbf{v})$ is nonconvex.

Overall, the reformulated optimization problem is given by

$$\begin{aligned} (\mathcal{P}2): \max_{t_0, \mathbf{u}, \mathbf{v}} \min_{m \in \mathcal{M}} \{ \log \tilde{R}_m(u_m, v_m) \} \\ \text{s.t. } t_0 > 0, \end{aligned} \quad (36a)$$

$$t_0 + \sum_{m=1}^M e^{u_m} \leq T_{\max}, \quad (36b)$$

$$v_m \leq \log P_{\max}, \quad \forall m \in \mathcal{M}, \quad (36c)$$

$$u_m + v_m \leq \log(E_m(t_0)), \quad \forall m \in \mathcal{M}, \quad (36d)$$

$$\tilde{F}_n(\mathbf{v}) \leq 0, \quad \forall n \in \mathcal{N}, \quad (36e)$$

where $\mathbf{u} \triangleq [u_1, \dots, u_M]^T \in \mathbb{R}^M$ and $\mathbf{v} \triangleq [v_1, \dots, v_M]^T \in \mathbb{R}^M$. Compared with the original problem ($\mathcal{P}1$), problem ($\mathcal{P}2$) is considerably more tractable due to the concave objective function and convex constraints, except for (36e). To tackle this issue, we construct suitable convex approximations and

Algorithm 1 Proposed Iterative Algorithm for $(\mathcal{P}1)$

Initialization

Initialize a feasible point $(t_0^{(0)}, \mathbf{u}^{(0)}, \mathbf{v}^{(0)})$, set iteration index $r = 0$ and threshold λ_{th} .

Iteration

a) Build $\tilde{F}_n^{(r)}(\mathbf{v})$ and corresponding convex problem $(\mathcal{P}2^{(r)})$ using $\mathbf{v}^{(r)}$;

b) Solve problem $(\mathcal{P}2^{(r)})$ to obtain $(t_0^{(r^*)}, \mathbf{u}^{(r^*)}, \mathbf{v}^{(r^*)})$;

c) If the relative objective improvement is below the threshold λ_{th}

Define $(t_0^*, \mathbf{u}^*, \mathbf{v}^*) = (t_0^{(r^*)}, \mathbf{u}^{(r^*)}, \mathbf{v}^{(r^*)})$ and go to d).

Else

Define $(t_0^{(r+1)}, \mathbf{u}^{(r+1)}, \mathbf{v}^{(r+1)}) = (t_0^{(r^*)}, \mathbf{u}^{(r^*)}, \mathbf{v}^{(r^*)})$, $r = r + 1$, and go back to a).

Reconstruction

d) Recover $t_m^* = e^{u_m^*}$ and $p_m^* = e^{v_m^*}$, $\forall m \in \mathcal{M}$, and calculate the corresponding objective value.

develop an SCA-based solution framework in the following subsection [17].

B. Iterative Algorithm

To handle the remaining nonconvexity in (36e), we adopt an SCA-based approach by constructing a convex surrogate of $\tilde{F}_n(\mathbf{v})$. At the r -th iteration, let $\mathbf{v}^{(r)}$ denote the current feasible point. Note that the nonconvexity of $\tilde{F}_n(\mathbf{v})$ stems from the last two concave terms. Since a concave function admits a global upper bound given by its first-order Taylor expansion, we upper-bound these concave terms at $\mathbf{v}^{(r)}$, which leads to an affine upper bound and thus a convex $\tilde{F}_n^{(r)}(\mathbf{v})$ satisfying $\tilde{F}_n(\mathbf{v}) \leq \tilde{F}_n^{(r)}(\mathbf{v})$ for all \mathbf{v} . The resulting surrogate is given in (37).

Accordingly, we obtain a convex optimization problem at iteration r as

$$\begin{aligned}
 (\mathcal{P}2^{(r)}): \quad & \max_{t_0, \mathbf{u}, \mathbf{v}} \quad \min_{m \in \mathcal{M}} \{ \log \tilde{R}_m(u_m, v_m) \} \\
 \text{s.t.} \quad & \tilde{F}_n^{(r)}(\mathbf{v}) \leq 0, \quad \forall n \in \mathcal{N}, \quad (38a) \\
 & (36a) - (36d),
 \end{aligned}$$

which can be easily solved using convex optimization tools. The inequality in (37) ensures that the constraint (38a) is always stricter than (36e), thus the feasible point in $(\mathcal{P}2^{(r)})$ is always feasible in $(\mathcal{P}2)$. The overall SCA-based iterative procedure is summarized in Algorithm 1.

IV. NUMERICAL RESULTS

In this section, numerical results are presented to evaluate the performance of the proposed wireless powered ISAC system. We consider an ISAC system consisting of one BS, $M = 10$ users, and $N = 10$ targets, where the BS is located at the origin and users as well as targets are randomly and independently distributed over a circular area of radius 10 m centered at the BS. The wireless channel gain is given by $h = z\kappa d^{-\nu}$, where d denotes the distance, $\kappa = 10^{-3}$ is the reference channel gain, $\nu = 2.5$ is the path loss exponent, and z represents a Rayleigh-distributed small-scale fading factor. Unless otherwise stated, the default simulation parameters are set as follows: $c = 3 \times 10^8$ m/s, $T_{\text{max}} = 10$ s, $p_0 = 10$ W, $P_{\text{max}} = 2$ W, $\sigma^2 = -70$ dBm, $\eta = 5 \times 10^{-2}$, $W = 1$ MHz, $\zeta_m = 0.7$, $\forall m \in \mathcal{M}$, and $\lambda_{\text{th}} = 10^{-5}$.

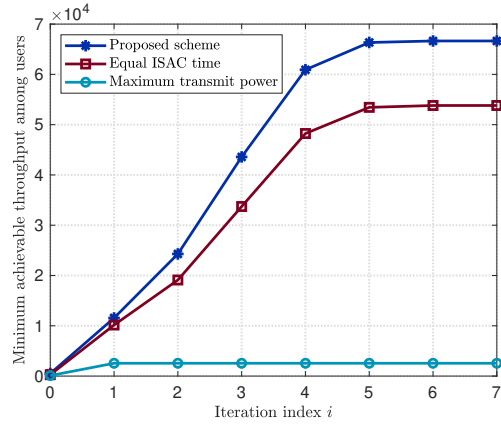


Fig. 2. Convergence behavior of the proposed and benchmark schemes.

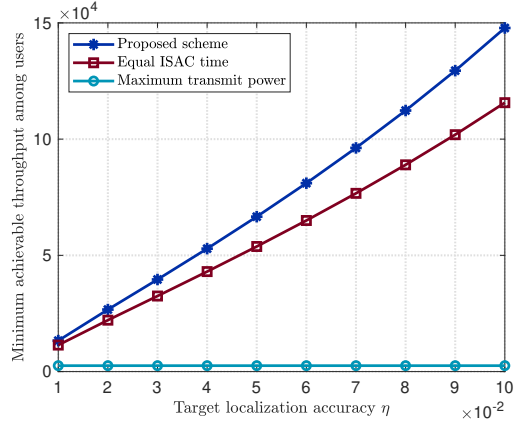


Fig. 3. Minimum achievable throughput versus target localization accuracy requirement.

To further demonstrate the effectiveness of the proposed joint resource allocation scheme, we provide the following two benchmark schemes for performance comparison:

- **Equal ISAC Time:** The total ISAC transmission duration is equally divided among all users, i.e., $t_m = t$, $\forall m \in \mathcal{M}$, while the variables (t_0, t, \mathbf{p}) are jointly optimized using a simplified variant of Algorithm 1.
- **Maximum Transmit Power:** All users transmit with the maximum allowable power, i.e., $p_m = P_{\text{max}}$, $\forall m \in \mathcal{M}$, while the variables (t_0, \mathbf{t}) are jointly optimized using a simplified variant of Algorithm 1.

At first, we examine the convergence behavior of the proposed iterative algorithm. Fig. 2 illustrates the evolution of the minimum achievable throughput among users versus the iteration index. It is observed that the proposed algorithm converges rapidly and stabilizes within a few iterations, demonstrating its reliability and efficiency. Compared with the benchmark schemes, the proposed method achieves a higher throughput.

Then, we evaluate how the system performance varies with the target localization accuracy requirement η . As shown in Fig. 3, the achievable throughput of both the proposed joint optimization scheme and the equal ISAC time scheme increases with η , since a higher η corresponds to a more relaxed localization constraint. In contrast, the maximum

$$\begin{aligned} \tilde{F}_n(\mathbf{v}) \leq & \sum_{m=1}^M \alpha_{m,n} e^{v_m} + \mu_n - \frac{\eta}{2} \sum_{i=1}^M \sum_{j=1}^M \beta_{i,j,n} e^{v_i^{(r)} + v_j^{(r)}} \left[1 + (v_i - v_i^{(r)}) + (v_j - v_j^{(r)}) \right] \\ & - \eta p_0 \sum_{m=1}^M \varphi_{m,n} e^{v_m^{(r)}} \left[1 + (v_m - v_m^{(r)}) \right] \triangleq \tilde{F}_n^{(r)}(\mathbf{v}), \quad \forall n \in \mathcal{N} \end{aligned} \quad (37)$$

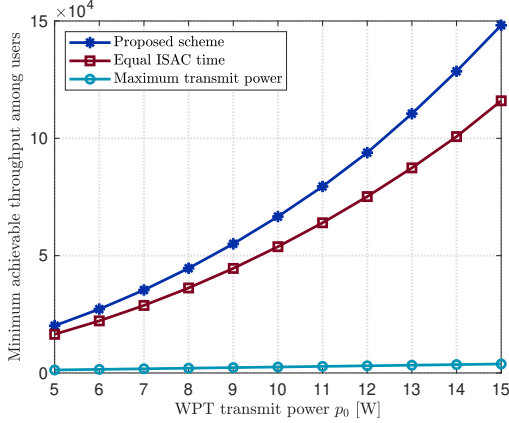


Fig. 4. Minimum achievable throughput versus WPT transmit power.

transmit power benchmark scheme remains insensitive to η whenever it is feasible, because the CRB constraint depends only on the fixed transmit powers and sensing geometry. When η is sufficiently small, the localization requirement cannot be satisfied under P_{\max} , and this benchmark becomes infeasible. Overall, the proposed method outperforms the benchmark schemes in varying localization requirements, highlighting the benefit of jointly optimizing the energy harvesting duration, ISAC transmission time, and transmit power.

Finally, we investigate the impact of the WPT transmit power on the achievable throughput. Fig. 4 shows the minimum achievable throughput among users as a function of the WPT transmit power p_0 . As p_0 increases, the achievable throughput of all schemes improves, since more energy can be harvested during the WPT phase to support subsequent ISAC transmissions under the same total time budget. The proposed method consistently outperforms the benchmark schemes over the entire range of p_0 , demonstrating the benefit of joint resource allocation. In contrast, the equal ISAC time scheme exhibits inferior performance due to its limited flexibility in time allocation. Moreover, the maximum transmit power scheme achieves significantly lower throughput since fixing the user transmit power reduces the degrees of freedom to balance energy harvesting, localization, and communication.

V. CONCLUSION

This paper investigates a wireless powered ISAC system with CRB-based target localization requirements. We propose a joint resource allocation framework that balances harvested energy, communication throughput, and localization accuracy. To tackle the resulting nonconvex problem, we first reformulate it via variable substitutions and logarithmic transformations, then develop an efficient SCA-based iterative algorithm. Numerical results demonstrate fast convergence

and consistent throughput gains over benchmark schemes under varying localization requirements and energy-harvesting conditions, highlighting the effectiveness of the proposed joint time and power allocation in wireless powered ISAC systems. The proposed framework paves the way for extensions to more general network architectures, such as multi-BS deployments and cooperative ISAC systems.

REFERENCES

- [1] S. Lu et al., "Integrated Sensing and Communications: Recent Advances and Ten Open Challenges," *IEEE Internet Things J.*, vol. 11, no. 11, pp. 19094-19120, Jun. 2024.
- [2] Y. Cui, F. Liu, X. Jing and J. Mu, "Integrating Sensing and Communications for Ubiquitous IoT: Applications, Trends, and Challenges," *IEEE Netw.*, vol. 35, no. 5, pp. 158-167, Sep. 2021.
- [3] S. Wang, W. Dai, H. Wang and G. Y. Li, "Robust Waveform Design for Integrated Sensing and Communication," *IEEE Trans. Signal Process.*, vol. 72, pp. 3122-3138, Jun. 2024.
- [4] P. Wang, D. Han, Y. Cao, W. Ni and D. Niyato, "Multi-Objective Optimization-Based Waveform Design for Multi-User and Multi-Target MIMO-ISAC Systems," *IEEE Trans. Wireless Commun.*, vol. 23, no. 10, pp. 15339-15352, Oct. 2024.
- [5] L. Sun, Z. Zhao, S. Wang, Z. Ding and M. Peng, "On the Study of Non-Orthogonal Multiple Access (NOMA)-Assisted Integrated Sensing and Communication (ISAC)," *IEEE Trans. Commun.*, vol. 72, no. 11, pp. 7278-7293, Nov. 2024.
- [6] F. Liu et al., "Integrated Sensing and Communications: Toward Dual-Functional Wireless Networks for 6G and Beyond," *IEEE J. Sel. Areas Commun.*, vol. 40, no. 6, pp. 1728-1767, Jun. 2022.
- [7] Z. Zhang et al., "Target Localization in Cooperative ISAC Systems: A Scheme Based on 5G NR OFDM Signals," *IEEE Trans. Commun.*, vol. 73, no. 5, pp. 3562-3578, May 2025.
- [8] X. Jing, F. Liu, C. Masouros and Y. Zeng, "ISAC From the Sky: UAV Trajectory Design for Joint Communication and Target Localization," *IEEE Trans. Wireless Commun.*, vol. 23, no. 10, pp. 12857-12872, Oct. 2024.
- [9] X. Li et al., "Integrating Sensing, Communication, and Power Transfer: From Theory to Practice," *IEEE Commun. Mag.*, vol. 62, no. 9, pp. 122-127, Sep. 2024.
- [10] Y. Chen, Z. Ren, J. Xu, Y. Zeng, D. W. K. Ng and S. Cui, "Integrated Sensing, Communication, and Powering: Toward Multi-Functional 6G Wireless Networks," *IEEE Commun. Mag.*, vol. 63, no. 8, pp. 146-153, Aug. 2025.
- [11] X. Li, Z. Han, Z. Zhou, Q. Zhang, K. Huang, and Y. Gong, "Wirelessly Powered Integrated Sensing and Communication," in *Proc. 1st ACM MobiCom Workshop ISCS*, Sydney, Australia, 2022, pp. 1-6.
- [12] O. Rezaei, M. M. Naghsh, S. M. Karbasi and M. M. Nayebi, "Resource Allocation for UAV-Enabled Integrated Sensing and Communication (ISAC) via Multi-Objective Optimization," in *Proc. IEEE Int. Conf. Acoust., Speech Signal Process. (ICASSP)*, Rhodes Island, Greece, 2023, pp. 1-5.
- [13] H. Godrich, A. Petropulu and H. V. Poor, "Power Allocation Schemes for Target Localization in Widely Distributed MIMO Radar Systems," in *Proc. IEEE Mil. Commun. Conf. (MILCOM)*, San Jose, CA, USA, 2010, pp. 846-851.
- [14] H. Godrich, A. P. Petropulu and H. V. Poor, "Power Allocation Strategies for Target Localization in Distributed Multiple-Radar Architectures," *IEEE Trans. Signal Process.*, vol. 59, no. 7, pp. 3226-3240, Jul. 2011.

- [15] X. Yuan, Y. Hu, M. Liu, T. Matsumura and A. Schmeink, "Optimal Beam Deployment for FSO Link Assisted Satellite-Ground Multicasting Communication," in *Proc. IEEE Wireless Commun. and Networking Conf. (WCNC)*, Milan, Italy, 2025, pp. 1-6.
- [16] P. Zheng, B. Li, X. Yuan, Y. Hu and A. Schmeink, "Multi-UAV-Enabled Cognitive Radio Networks: Joint UAV Deployment and Resource Allocation Design," in *Proc. 28th Int. Workshop Smart Antennas (WSA)*, Erlangen, Germany, 2025, pp. 208-213.
- [17] G. Scutari and Y. Sun, "Parallel and Distributed Successive Convex Approximation Methods for Big-Data Optimization," in *Multi-Agent Optimization*. Cham, Switzerland: Springer, Jan. 2018, pp. 141-308.